

# A Type of Buckling Restrained Brace for Convenient Inspection and Replacement



**15 WCEE**  
LISBOA 2012

**An-Chien Wu & Pao-Chun Lin**

National Center for Research on Earthquake Engineering, Taipei, Taiwan

**Keh-Chyuan Tsai**

National Taiwan University, Taipei, Taiwan

## SUMMARY:

In this study, cyclic loading tests on three novel all-steel buckling restrained braces (BRBs) are conducted to investigate the high mode buckling phenomenon. The proposed BRB is composed of a steel core plate and two identical restraining members which restrain the core plate using shim spacers. The proposed BRBs can be visually inspected following a major earthquake. The two restraining members can be conveniently disassembled and the damaged core plate can be replaced if necessary. Tests confirm that the larger the applied axial compressive strain is, the shorter the high mode buckling wave length would develop. The weak-axis buckling wave length is about 12 times the core plate thickness when a core compressive strain of 3.5% is reached. Tests indicate that the proposed BRBs can effectively sustain large cyclic strain reversals. The high mode buckling wave length can be satisfactorily predicated using the proposed method.

*Keywords:* buckling restrained brace, restraining member, high mode buckling, wave length, local failure

## 1. INTRODUCTION

In contrast to the behavior of buckling braces, BRBs can be designed and fabricated to sustain yielding in both tension and compression (Watanabe *et al.* 1988). Therefore, BRBs have been increasingly adopted as hysteretic dampers to improve the earthquake resisting performance of the building and bridge structures (Uang *et al.* 2004, Tsai *et al.* 2008, Tsai and Hsiao 2008). A typical BRB has the core member encased by the buckling restrainer so that the failure of the core member cannot be easily detected. When the core member is subjected to the compression, the buckling restrainer must provide sufficient stiffness to prevent overall flexural buckling of the BRB (Watanabe *et al.* 1988). Lateral expansion increases the core member section due to Poisson effect under such compression. Thus, the clearance must be devised between the core member and the buckling restrainer to minimize the friction transferred to the restrainer (Watanabe *et al.* 1988, Wu *et al.* 2011). The clearance allows the core member to buckle first and the high mode buckling wave may form soon after the core member goes into the plastic range. The outward high mode buckling force is then produced at the crest of the high mode buckling wave (Wu *et al.* 2011, Lin *et al.* 2012). The restrainer local failure could occur due to the high mode buckling of the core member when the restrainer is not strong enough (Takeuchi *et al.* 2010, Lin *et al.* 2012). Takeuchi *et al.* carried out experimental and numerical analyses of mortar-filled BRBs to propose a criterion for the local restraint failure due to the core plate strong-axis buckling. Chou and Chen also presented the design recommendation for the sandwiched BRB to prevent the global and local buckling. Lin *et al.* provided the recommendation on the seismic design of thin BRB steel casing against local bulging failure.

Strong aftershocks could occur following the main shocks. In order to guarantee effective seismic performance of the buckling-restrained braced frames (BRBFs) which might experience multiple earthquakes and aftershocks during the service life, developing the technique for inspecting BRBs is warranted. Previous researchers have based on such concepts for BRBs in which the restrainers could be disassembled first for inspection of the core member (Takeuchi *et al.* 2010, Chou and Chen 2010).

After the inspection, however, the restrainer is difficult to be reintegrated with the core member where large plastic deformations have taken place. Thus, after a major earthquake, it would be desirable if the condition of the core plate could be visually inspected without disassembling any part of the BRBs. The proposed BRB is composed of a steel core plate and two identical restraining members which restrain the core plate by bolts at a specific spacing. The strength of the bolts must be sufficient to resist the outward high mode buckling forces developed during the weak-axis high mode buckling of the core plate. In addition, the spacing of the bolts must be smaller than the strong-axis buckling wave length of the core member. Shim spacers are arranged to allow the development and observation of the high mode core plate buckling. The proposed BRBs can be visually inspected following a major earthquake. The two restraining members can be conveniently disassembled and the damaged core plate can be replaced if necessary. In this study, cyclic loading tests on three all-steel BRBs are conducted using various loading protocols on two different cross sections of the core plate to investigate the high mode buckling phenomenon. The relationships among the core plate high mode buckling wave length, clearance between the core plate and buckling restrainer, and the outward pushing forces are investigated through the experiments.

## 2. CONCEPTS OF THE BRBS FOR CONVENIENT INSPECTION AND REPLACEMENT

Figure 2.1 shows the novel BRB for immediate inspection and convenient replacement following the earthquakes. Two identical restraining members are formed by welding a steel channel to a flat plate. The core plate (Fig. 2.1a) is sandwiched by the two restrainers (Fig. 2.1b) using the high strength bolts. Special spacers (Figs. 2.1b, 2.1c and 2.1e) slightly thicker than the core plate are carefully arranged to provide the needed clearances between the core plate and restrainers in both strong and weak axis directions. The clearance  $s_s$  is the gap between the core plate edge to the spacer while  $s_w$  is the clearance between the surface of the core plate and the restraining members as shown in Fig. 2.1e. This allows the convenient inspecting of the core plate condition. Two key limit states governing the proposed BRB design are to prevent the global flexural buckling and local flexural failures of the restraining member. Five main issues are discussed as follows:

### 1. Global flexural buckling

In order to prevent the global flexural failure of the BRB, the critical load of the restrainer must be greater than the BRB maximum compressive strength. The critical load is estimated using the Euler theory of buckling:

$$P_{cr} = \frac{\pi^2 E_{sc} I_{sc}}{L_{sc}^2} \quad (2.1)$$

where  $E_{sc}$  and  $I_{sc}$  are the elastic Young's modulus and the moment of inertia about the weak-axis of the restraining member, respectively; and  $L_{sc}$  is the length of the restrainer (Fig. 2.1b).

### 2. Strong-axis high mode buckling wave length

The clearances between the core plate and the restraining members lead to the high mode buckling in both the strong and weak axes of the core plate when the restraining member has sufficient flexural strength. The strong-axis high mode buckling wave length,  $L_s$ , can be approximated by applying the Euler formula with the BRB yield strength  $P_y$ :

$$L_s = \sqrt{\frac{4\pi^2 (EI)_{eff}}{P_y}} \quad (2.2)$$

where  $(EI)_{eff}$  is the equivalent flexural stiffness with a multiple of the elastic flexural stiffness of the core plate  $EI_s$ . The  $E$  and  $I_s$  are the elastic Young's modulus and the strong-axis moment of inertia of the core plate, respectively. This strong-axis high mode buckling wave length (Takeuchi *et al.* 2010)

can be determined by the width of the core plate,  $w_c$ , and the tangent modulus in the plastic range. Takeuchi *et al.* suggested that the tangent modulus equals to 2% of the elastic Young's modulus, i.e.  $(EI)_{eff} = 0.02EI_s$ , could be used to approximate the strong-axis high mode buckling wave length. The peak compressive strength of the BRB is expected to be higher than the yield strength  $P_y$  due to the strain hardening and friction force developed between the core plate and the restrainer.

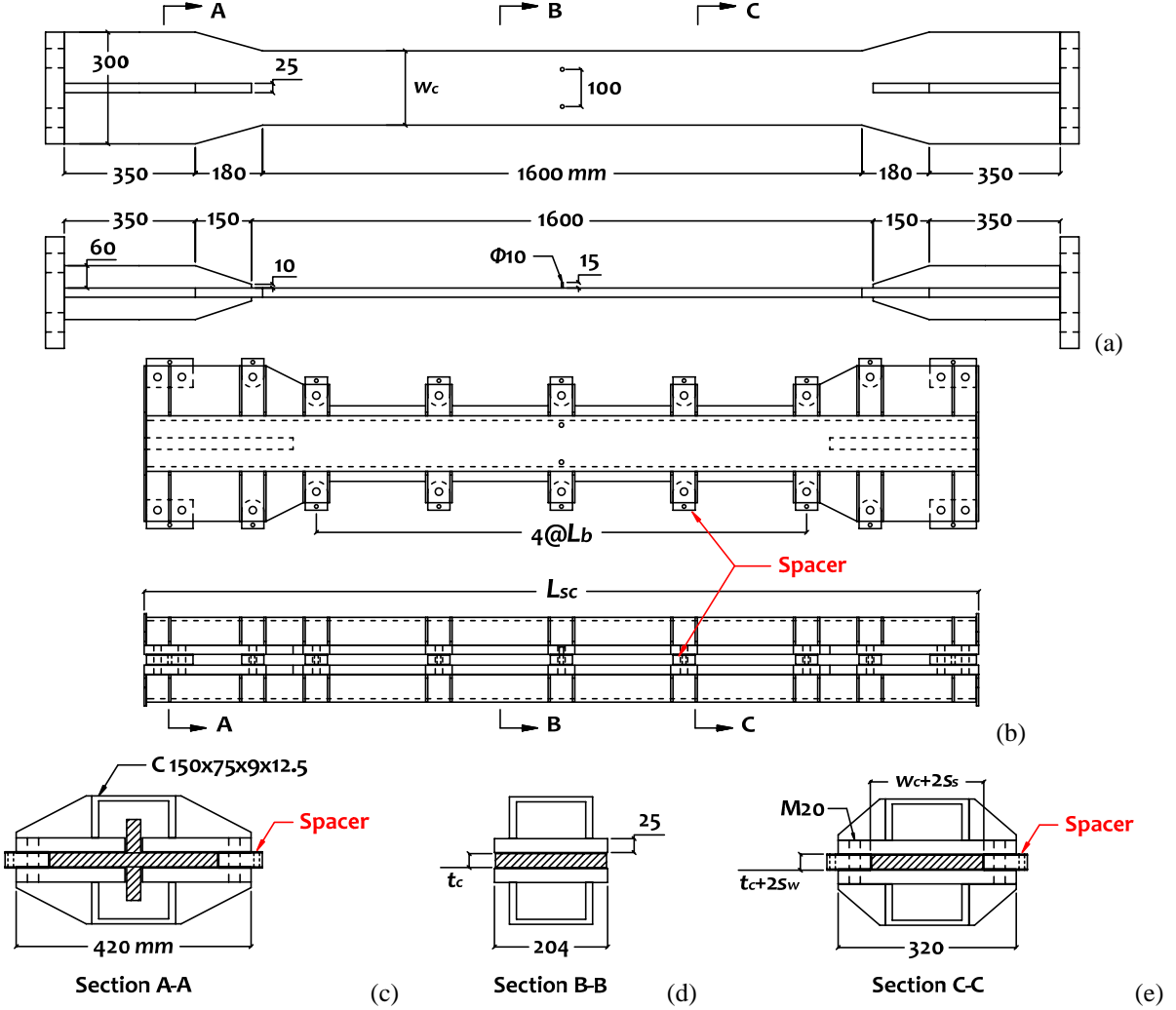


**Figure 2.1.** Profiles of the proposed buckling restrained brace

### 3. Forces acting on spacers and bolts

When the BRB is subjected to the tension force, the width of the core plate decreases by  $v\varepsilon_c w_c$ , where  $v = 0.5$  is the plastic Poisson ratio. The clearance between the core plate and the spacer increases by half of this value. Thus, as illustrated in Fig. 2.2, the force  $N_s$  acting on the spacer and bolt can be estimated according to the geometric relationship between the strong-axis high mode buckling wave length and the core plate edge clearance  $s_s$  as:

$$N_s = \frac{4s_s + 2v\varepsilon_c w_c}{L_s} P_{\max} \quad (2.3)$$

where  $\varepsilon_c$  and  $P_{\max}$  are the expected core plate maximum tensile strain and BRB compressive strength, respectively. In the restrainer design, the spacing  $L_b$  of the bolted spacer must be no greater than one half of the wave length in order to resist the outward high mode buckling forces in the strong-axis. The shear strength of the clamping bolt needs to sustain this force  $N_s$ . Additional tension force on the bolts due to the weak-axis high mode buckling will be discussed later.

#### 4. Weak-axis high mode buckling wave length

During the weak-axis high mode buckling, the core plate goes into a more significant plastic flexural condition with a greater strain reversal. Thus, it is considered that part of the cross-section is unloaded in the elastic manner. The Shanley's double modulus theory (Shanley 1946) has been adopted to take the loading and unloading phenomenon into account (Lin *et al.* 2012). The effective flexural stiffness can be calculated as:

$$(EI)_{eff} = E_t \int_0^{t_c/2-c} x^2 w_c dx + E \int_0^{t_c/2+c} x^2 w_c dx \quad (2.4)$$

where  $E_t$  is the post yield Young's modulus and  $c$  is the distance from the center line to the neutral axis of the core plate as illustrated in Fig. 2.3. According to the previous test results (Lin *et al.* 2012), the  $E_t$  is about 2.5% of  $E$ , and 15% of the core cross section area goes into unloading stage. Thus, an approximate equivalent flexural stiffness of 10% of the elastic flexural stiffness,  $(EI)_{eff} = 0.10EI_w$ , can be obtained, where  $I_w$  is the core plate weak-axis moment of inertia. The weak-axis high mode buckling wave length,  $L_w$ , could be approximately computed from the right hand side of Eqn. 2.2 using  $(EI)_{eff} = 0.10EI_w$ . The high mode buckling wave length for the CNS SN490B steel with a nominal yield strength of 325MPa is about 12 times the core thickness  $t_c$ .

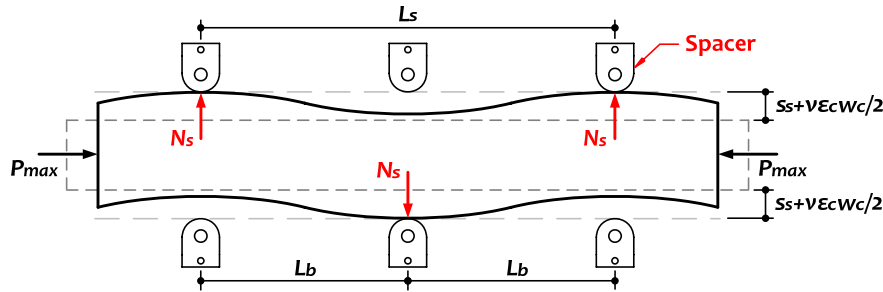


**Figure 2.2.** Strong-axis high mode buckling of the core plate

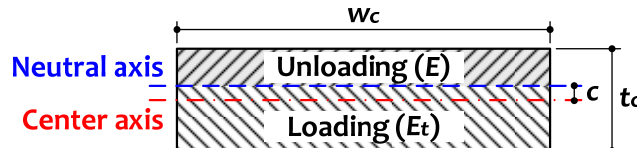


**Figure 2.3.** Loading and unloading regions in the core plate

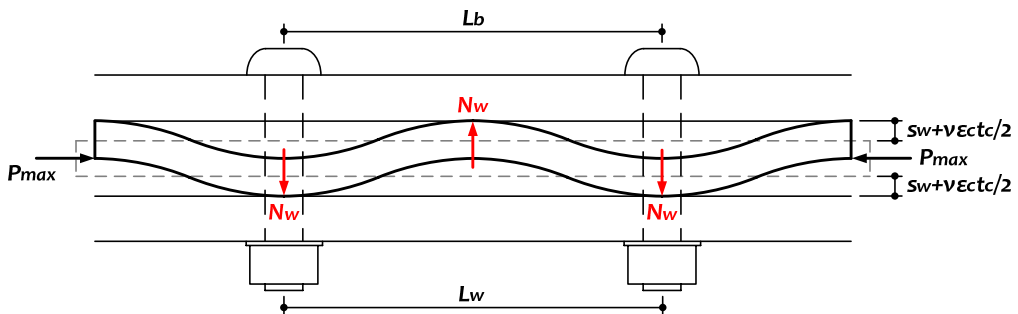


**Figure 2.4.** Weak-axis high mode buckling of the core plate

#### 5. Forces acting on restraining members

As mentioned in issue 3, the clearance between the core plate and the restrainer also increases by one half of  $v\epsilon_c t_c$  in the tensile stage. As shown in Fig. 2.4, the force  $N_w$  acting on the restraining member can be expressed in the similar manner stated above:

$$N_w = \frac{4s_w + 2\nu\varepsilon_c t_c}{L_w} P_{\max} \quad (2.5)$$

When a pin-supported boundary condition is assumed at the bolted spacer locations, the maximum bending moment in a restraining member can be computed by arranging the most critical acting forces  $N_w$  between the two bolted spacers. The number of the acting forces depends on the wave length  $L_w$  and the longitudinal distance of the spacers. The elastic flexural stiffness and strength provided by any one of the restraining members must be sufficient. In addition, the clamping bolt must have the ability to resist the acting forces  $N_w$  between the spacers.

### 3. TEST PROGRAM

As mentioned in issues 2 to 5, it is evident that the core plate high mode buckling wave length is critical to the magnitude of the outward high mode buckling force (Lin *et al.* 2012). Thus, one of the main objectives of this experiment is to gain insights into the formation of the buckling and variations of the wave length as the axial strain changes.

#### 3.1. Specimens

Details of specimen dimensions and cross-sectional profiles are shown in Fig. 2.1. Table 3.1 summarizes each specimen dimensions and coupon test results of core plates. The core member and spacers were made of CNS SN490B steel. At the center of the core plate, two stopper pins of 10mm diameter and 15mm high were welded to the core plate surface to prevent the relative longitudinal movement between the core plate center cross section and the restraining members. Each of the two restraining members mainly consisted of an A36 25mm thick steel plate and a 150×75×9×12.5mm channel (Fig. 2.1). Two restraining members were clamped by 20mm diameter S10T tensioned high-strength bolts at specific spacing. Spacers were designed to allow 1mm clearance  $s_w$  between the core plate and restraining member, and a 2mm clearance  $s_s$  between the core plate and itself. In order to reuse the restraining members for all three BRB specimens, the restraining members were conservatively designed meeting all the requirements described in Section 2. Spacers were arranged with the spacing  $L_b$  (Table 3.1 and Fig. 2.1b) for monitoring the variation of the core plate high mode buckling wave length during the tests.

**Table 3.1.** Dimensions and coupon test results of the core plates

Specimen	$w_c$ (mm)	$t_c$ (mm)	$F_y$ (MPa)	$s_s$ (mm)	$s_w$ (mm)	$L_{sc}$ (mm)	$L_b$ (mm)
w160t20-1	160	20	344	2	1	2260	332
w160t20-2							
w200t20-1	200						

#### 3.2. Test setup and loading protocol

As shown in Fig. 3.1, a 4900kN capacity universal testing frame was used in the experiments. Each end of the core member was welded to an end plate before connecting to the testing frame. The cyclic axial displacements were applied along the BRB axis. The axial forces were measured by a load cell. The axial displacements of the specimen were measured by two displacement transducers installed at both ends of the specimen. In order to monitor the outward deformations between the two restraining members when the high mode buckling bulging forces developed, four additional displacement gauges (Fig. 3.1) were mounted at the mid-point between the two adjacent spacers in the longitudinal direction. Two tape measures were attached to the edges of the restraining member (Fig. 3.2). Each side of the core plate was painted using yellow color for convenient observing and recording the variations of the high mode buckling wave length formation during the tests as shown in Fig. 3.2.

It was anticipated that the BRB core plate high mode buckling wave length varied with the changing core strains. The possible shortest wave length should be related to the largest compressive core strain.

In order to investigate the effects of the strain history on the variation of the wave length, three different loading protocols as shown in Fig. 3.3 were applied in the experiments. All specimens were subjected to a cyclic increasing or decreasing axial strains followed by a cyclic constant fatigue strains until the specimen failed. Fig. 3.3 also shows that the tensile or compressive yield strain  $\varepsilon_y$  was applied first for all specimens. Specimen w160t20-1 was conducted with cyclically increasing strains with tensile strain applied first in each of the two cycles, ranging from 0.5% to a maximum 3.5% with an increment of 0.5%. Specimen w160t20-2 was conducted with cyclically decreasing strains with compressive strain applied first in each of the two cycles, starting from 3.5% to 0.5% with a decrement of 0.5%. Specimen w200t20-1 adopted cyclically decreasing strains starting from a peak tensile 3.0% strain applied first down to 1.0% with a decrement of 1.0% in each of the two cycles. For all specimens, cyclic fatigue strains (Fig. 3.3) were then applied using a 2.0% core strain until failure. During the cyclically increasing or decreasing strains, the actuator displacement was held at each compressive strain peak to measure the high mode buckling wave length.



**Figure 3.1.** Test setup



**Figure 3.2.** Experimental observations of the high mode buckling wave length

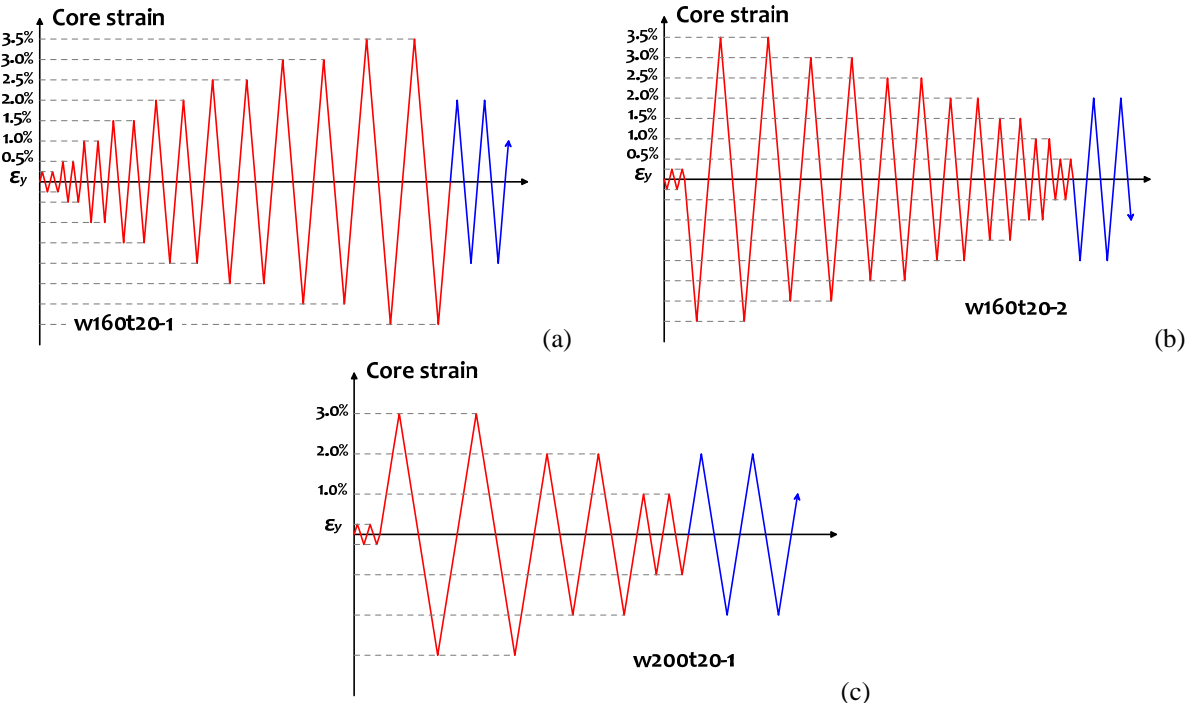


**Figure 3.3.** Loading protocols for Specimens (a) w160t20-1, (b) w160t20-2, and (c) w200t20-1

### 3.3. Test result

The cyclic force versus deformation hysteretic responses for all three specimens are shown in Figs. 3.4 to 3.6. When the first yield strain cycle was applied for w160t20-1, weak-axis high mode buckling waves formed evidently with a relatively large wave length (Table 3.2). As cyclic strains increased, it was observed that the larger the compressive strain is applied, the more waves and the shorter high mode buckling wave length forms. However, at the same two cyclic peak compressive strain levels, approximately the same wave shape and lengths were observed (Table 3.2). After the 2.5% cyclic peak compressive strain was applied, the high mode buckling wave was found keeping almost the same shape and with an average wave length of 240mm (or 12 times the core plate thickness) even when the 3.5% peak compressive strain was reached. When the cyclic increasing strain cycles were completed, the stopper failed and separated from the core plate on the first tension excursion of the fatigue strain. As a result, the restrainer slid down and almost hit the bottom end plate. In order to reuse the restrainer for future tests, test was stopped to prevent possible damage to the restrainer. The core plate was never fractured.

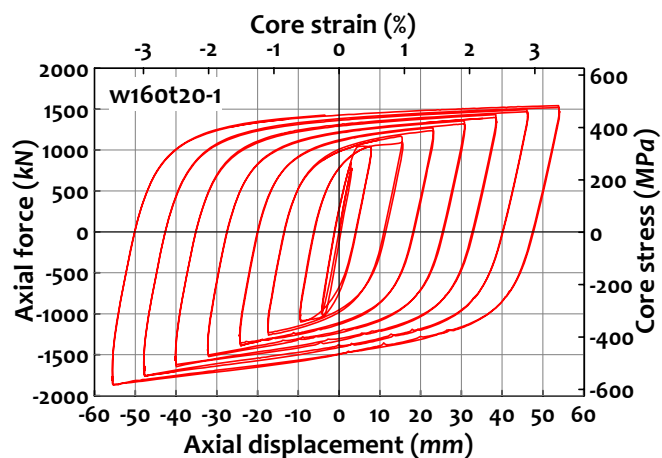


**Figure 3.4.** Hysteretic response of Specimen w160t20-1

In w160t20-2 test, when the first 3.5% compressive strain was imposed following the application of the yield strain, the weak-axis high mode buckling waves formed with an average wave length of about 241mm (Table 3.2). Again, due to the separation of the stoppers from the core plate, the restrainer started to slide slightly at the 6<sup>th</sup> cycle fatigue strain. This led to a sudden increase of the compressive strength as shown in Fig. 3.5. As the test continued, the core plate eventually fractured at the 9<sup>th</sup> cycle fatigue strain. As shown in Fig. 3.7a, the core plate fractured condition was easily observed on site without taking the restrainers apart.

**Table 3.2.** Experimental average core plate high mode buckling wave lengths

Specimen	$\varepsilon_y$	Wave length at various peak strain levels (mm)						
		0.5%	1.0%	1.5%	2.0%	2.5%	3.0%	3.5%
w160t20-1	940	665	385	245	245	245	240	240
w160t20-2	603	241	241	241	241	241	241	241
w200t20-1	1160	-	225	-	225	-	225	-

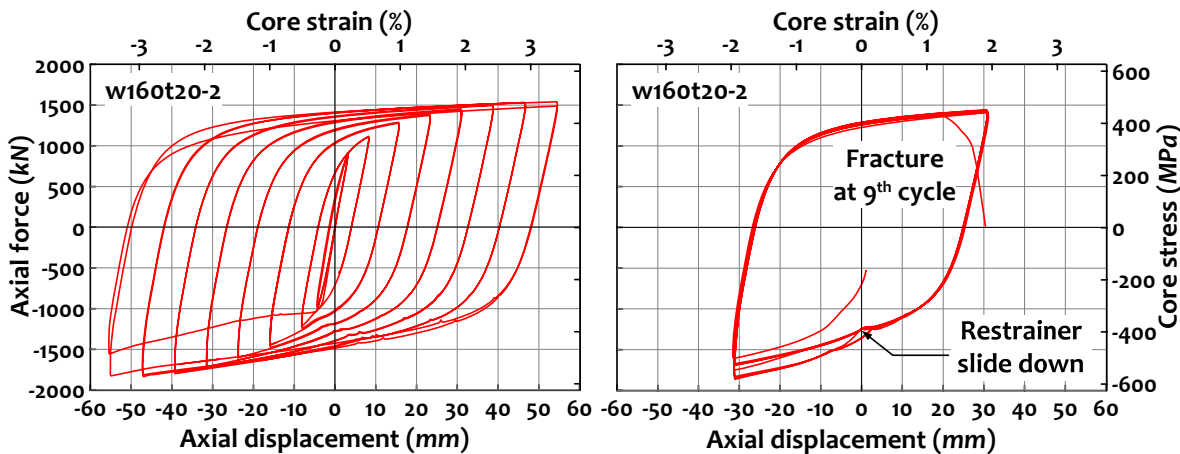


**Figure 3.5.** Hysteretic responses of Specimen w160t20-2

The weak-axis buckling of the w200t20-1 core plate formed with an average wave length of 225mm when the first compressive strain of 3.0% was applied. The buckling wave shape and length were maintained almost the same during the rest of the test (Table 3.2). Its core plate fractured at the 39<sup>th</sup> cycle fatigue strain. The fracture condition is shown in Fig. 3.7b.

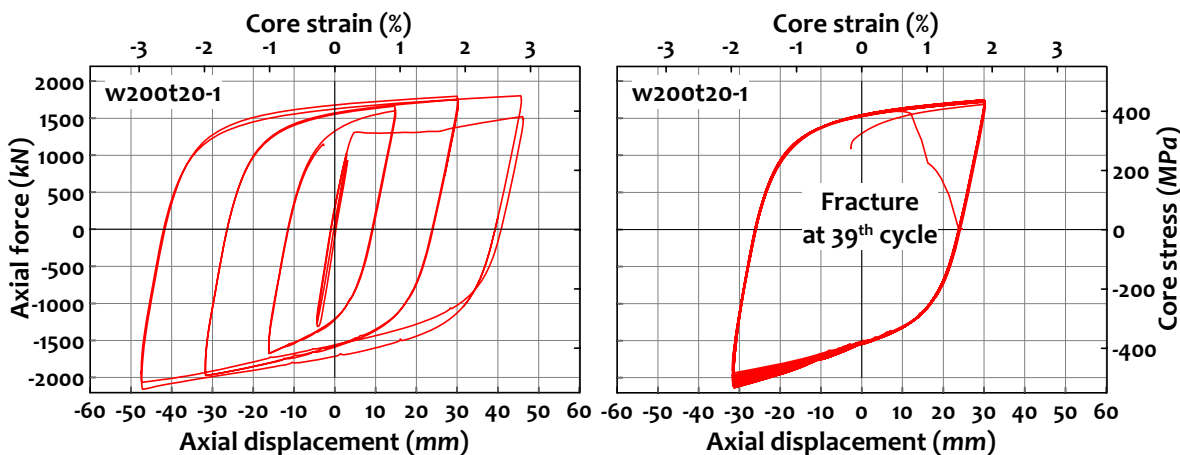


**Figure 3.6.** Hysteretic responses of Specimen w200t20-1

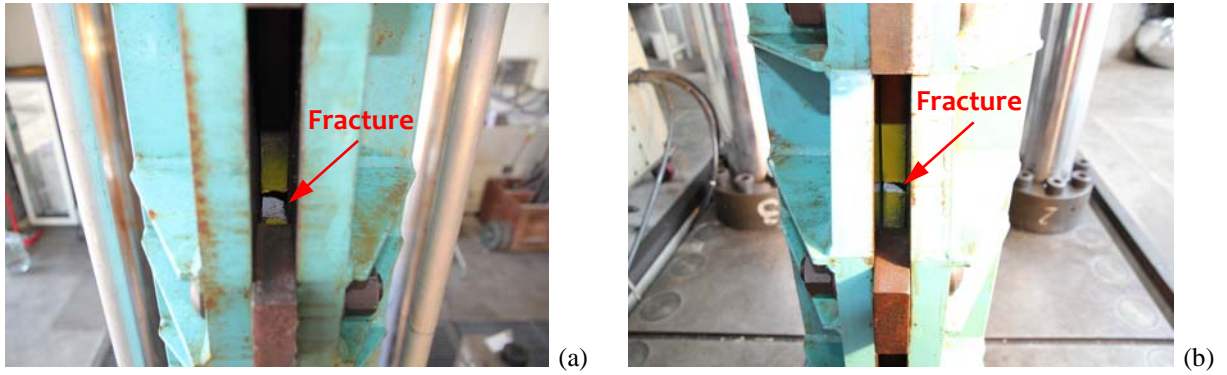


**Figure 3.7.** Core plate fracture of Specimens (a) w160t20-2, and (b) w200t20-1

As shown in Figs. 3.4 to 3.6, all specimens exhibited stable hysteretic behavior regardless the variations of the loading protocol. The peak outward deformation between the two restraining members was less than 0.4mm during the tests of all specimens. From the experimental results, the ratios between the peak compressive and tensile strengths at each strain level (the strength adjustment,  $\beta$  factor) were tabulated in Table 3.3 and plotted in Fig. 3.8. It is evident that the  $\beta$  factors for all specimens are less than 1.22, suggesting these BRBs are of good quality in preventing excessive friction built-up between the core and the restrainer. In addition, the cumulative plastic deformations (CPDs) for specimens are 446, 701 and 1326, times the yield strain, as indicated in Table 3.3. In all three tests, no evident strong-axis buckling of the core plate was observed.

**Table 3.3.** Experimental  $\beta$  factors and CPDs

Specimen	$\beta$ factors at various strain levels							CPD
	0.5%	1.0%	1.5%	2.0%	2.5%	3.0%	3.5%	
w160t20-1	1.03	1.11	1.09	1.13	1.15	1.19	1.22	446
	1.04	1.06	1.09	1.11	1.13	1.17	1.21	
w160t20-2	1.12	1.15	1.17	1.19	1.20	1.18	1.04	701
	1.09	1.13	1.16	1.18	1.20	1.20	1.18	
w200t20-1	-	1.00	-	1.09	-	-	-	1326
		1.03	-	1.12	-	1.19	-	

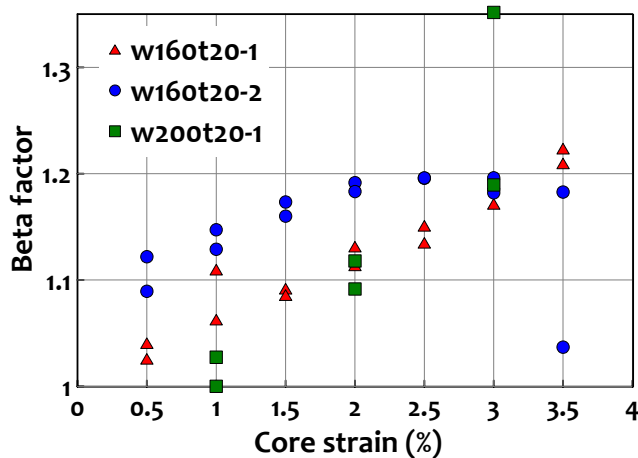


**Figure 3.8.** Experimental  $\beta$  factors at various core strain levels

#### 4. CONCLUSIONS

1. A novel BRB for immediate inspection and convenient replacement is proposed. The design of proposed BRB works effectively and the BRB core plate high mode buckling responses could be observed easily without disassembling the restraining member during the tests. Test confirms that

- the proposed restrainer could be reused. It allows the BRB with different core plate cross sectional dimensions to develop full hysteresis responses.
2. The maximum core strains of Specimens w160t20-1 and w160t20-2 reached 3.5% and the Specimen w200t20-1 reached 3.0%. These specimens all had good energy absorption performance with a CPD capacity reached 446, 701, and 1326 for Specimen w160t20-1, w160t20-2, and w200t20-1, respectively.
  3. The ratios between the experimental cyclic peak compressive and tensile strengths are smaller than 1.22 for all specimens. It shows these BRBs are of good quality in preventing excessive friction built-up between the core and the restrainer.
  4. Tests confirm that the larger the applied axial compressive strain is, the shorter the high mode buckling wave length would develop. The wave lengths will not increase if the subsequent applied compressive strain is smaller than the previous one.
  5. Test results show that the BRB flat core plate high mode buckling wave lengths range from 225 to 240mm. It can be satisfactorily predicted using the proposed method.
  6. Although the experimental peak tensile and compressive strains reached during the tests (3.0%~3.5%) are considered very large, this series of tests provide a good data base for the conservative estimate of the possible outward pushing force caused by the core plate high mode buckling.

#### **ACKNOWLEDGEMENT**

The financial supports from the Taiwan National Science Council and the National Center for Research on Earthquake Engineering (NCREE) are much appreciated. The associate research fellow Jia-Chian Chen from NCREE participated in the tests. The excellent technical supports provided by NCREE are extremely instrumental to the success of these tests.

#### **REFERENCES**

- Chou, C.C. and Chen, S.Y. (2010). Subassemblage tests and finite element analyses of sandwiched buckling-restrained braces. *Engineering Structures*. **32:8**, 2108-2121.
- Lin, P.C., Tsai, K.C., Wang, K.J., Yu, Y.J., Wei, C.Y., Wu, A.C., Tsai, C.Y., Lin, C.H., Chen, J.C., Schellenberg, A.H., Mahin, S.A. and Roeder, C.W. (2012). Seismic design and hybrid tests of a full-scale three-story buckling-restrained braced frame using welded end connections and thin profile. *Earthquake Engineering and Structural Dynamics*. **41:5**, 1001-1020.
- Shanley, F.R. (1946). The column paradox. *Journal of the Aeronautical Sciences*. **13:12**, 768.
- Takeuchi, T., Hajjar, J.F., Matsui, R., Nishimoto, K. and Aiken, I.D. (2010). Local buckling restraint condition for core plates in buckling restrained braces. *Journal of Constructional Steel Research*. **66:2**, 139-149.
- Tsai, K.C., Hsiao, P.C., Wang, K.J., Weng, Y.T., Lin, M.L., Lin, K.C., Chen, C.H., Lai, J.W. and Lin, S.L. (2008). Pseudo-dynamic tests of a full-scale CFT/BRB frame-Part I: Specimen design, experiment and analysis. *Earthquake Engineering and Structural Dynamics*. **37:7**, 1081-1098.
- Tsai, K.C. and Hsiao, P.C. (2008). Pseudo-dynamic tests of a full-scale CFT/BRB frame-Part II: Seismic performance of buckling-restrained braces and connections. *Earthquake Engineering and Structural Dynamics*. **37:7**, 1099-1115.
- Uang, C.M., Nakashima, M. and Tsai, K.C. (2004). Research and application of buckling-restrained braced frames. *Steel Structures*. **4**, 301-313.
- Watanabe, A., Hitomi, Y., Saeki, E., Wada, A. and Fujimoto, M. (1988). Properties of brace encased in buckling-restraining concrete and steel tube. *Proceedings of the 9th World Conference on Earthquake Engineering*. **IV**: 719-724.
- Wu, A.C., Wei, C.Y., Lin, P.C. and Tsai, K.C. (2011). Experimental investigations of welded end-slot connection and unbonding layers for buckling restrained braces. *The 6th International Symposium on Steel Structures*. 587-594.